Proceedings of the International Conference on Oxide Materials for Electronic Engineering, May 29–June 2, 2017, Lviv

Ionic Conductivity in Multiphase Li_2O-$7GeO_2$ Compounds

O.O. Nesterov[a], M.P. Trubitsyn[a,*], S.G. Nedilko[b], M.D. Volnianskii[a], S.M. Plyaka[a] and Ya.O. Rybak[b]

[a]Oles'Honchar Dnipro National University, prosp. Gagarina 72, Dnipro, 49010, Ukraine

[b]Taras Shevchenko National University of Kyiv, 64/13 Volodymyrska Str., Kyiv, 01601, Ukraine

Crystallization of Li_2O–$7GeO_2$ glass was carried out on heating, simultaneously differential scanning calorimetry and electric properties were studied. Morphology of the phase states obtained at glass devitrification was examined by atomic force microscopy. It was shown that amorphous phase of Li_2O–$7GeO_2$ was crystallized in stages through the intermediate state with increased conductivity σ. In the intermediate state the sample volume was occupied by nanometer-sized nuclei with ordered structure surrounded by internuclear amorphous medium. Complete glass crystallization occurred through transformation of nanometer-sized nuclei into micrometer-sized crystallites and was accompanied by a sharp and irreversible decrease of conductivity. Atomic force microscopy of the samples heat-treated in different ways showed that Li_2O–$7GeO_2$ glass crystallization was suppressed near the surface and mainly proceeded within the sample bulk. Charge transfer in amorphous, nanocrystalline intermediate and polycrystalline phases of Li_2O–$7GeO_2$ was associated with motion of the weakly bound Li ions.

DOI: 10.12693/APhysPolA.133.892

PACS/topics: 61.43.–j, 66.10.Ed, 77.84.–s, 68.37.Ps

1. Introduction

The current trend in development of new functional materials is associated with spatially inhomogeneous multiphase compounds. In addition to chemical composition and atomic structure, the essential factors for such materials are relative volume and mean size of the homogeneous regions as well as the type of their spatial distribution [1, 2].

Lithium heptagermanate $Li_2Ge_7O_{15}$ belongs to the family of Li_2O–$x GeO_2$ compounds [3], which have promising applications as new solid electrolytes. The framework of the $Li_2Ge_7O_{15}$ crystal structure is formed by germanium–oxygen octahedra [GeO_6] and tetrahedra [GeO_4], which are connected by bridge oxygen atoms [4–6]. Li^+ ions are located within the structural channels, formed by germanium–oxygen lattice framework, and compensate its negative charge. Study of conductivity σ in Li_2O–$x GeO_2$ polycrystals [7] demonstrated that σ depended on chemical composition and increased in compounds with higher fraction of Li_2O. Studies of pure and doped $Li_2Ge_7O_{15}$ single crystals evidenced that charge transfer in lithium heptagermanate was determined by Li interstitials hopping along the structural channels [8–11].

Preparation of the Li_2O–$x GeO$ glasses and their devitrification on heating was reported in [12–17]. It was shown that with increasing temperature the amorphous compounds with $x>3$ crystallized in stages through intermediate state. In Refs. [18–20] it was revealed that the intermediate state in the Li_2O–$x GeO$ (x = 7, 11.5) was metastable and characterized by increased electrical conductivity.

*corresponding author; e-mail: trubitsyn_m@ua.fm

In this paper, we studied temperature behavior of conductivity σ in AC field during Li_2O–$7GeO_2$ glass crystallization occurred upon heating. Devitrification of amorphous phase was examined by differential scanning calorimetry (DSC). Morphology of the phase states, obtained at glass crystallization, was tested by atomic force microscopy (AFM).

2. Experimental

Li_2O–$7GeO_2$ glass was prepared by the melt quenching in accordance with the procedure described in [16]. DSC was performed on a Mettler STAReSW derivatograph in the temperature range 290–1200 K on the first heating run carried out with the rate 10 K/min. For DSC measurements the pieces of glass were ground into a powder. Conductivity σ was measured in AC field (f = 1 kHz) by a bridge method in the interval 300–950 K on heating with the average rate close to that used in DSC experiment. The samples for σ measurements were prepared as plane-parallel plates with dimensions 5×5 mm^2 and thickness of about 1 mm. The Pt electrodes were deposited in vacuum on the samples main planes. AFM images were obtained by using the Integra Prima Basic NT-MDT microscope at room temperature. The surfaces for AFM imaging were prepared by cleaving the pieces of glass or heat treated samples. All experiments were performed in air at normal atmospheric pressure and humidity.

3. Results and discussion

3.1. Calorimetry of glass crystallization

DSC curve, measured on the first heating run of the Li_2O–$7GeO_2$ glass, is shown in Fig. 1. In accordance with the data reported in [12–16], the DSC curve reveals the inflection point at glass transition temperature (T_g =

775 K) and two exothermic peaks observed at $T_1 = 840$ K and $T_2 = 910$ K. One has to note that DSC anomalies, shown in Fig. 1, can be detected only for the first heating run of as-quenched glass. After heating above T_2 the Li_2O–$7GeO_2$ glass was completely crystallized and DSC measuring did not reveal any anomalies in subsequent cooling and heating cycles.

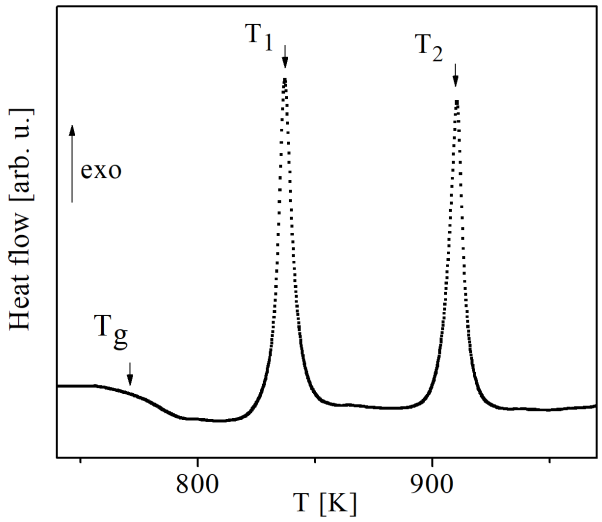

Fig. 1. DSC curve obtained on the first heating run of Li_2O–$7GeO_2$ glass. Inflection point corresponds to glass transition temperature $T_g = 775$ K. Exothermic peaks at $T_1 = 840$ K and $T_2 = 910$ K demonstrate that glass crystallizes in stages. Heating rate was 10 K/min.

Presence of two DSC peaks demonstrates that amorphous phase of Li_2O–$7GeO_2$ crystallizes in two stages. Structures of the phases crystallized at T_1 and T_2 were studied by X-ray phase analysis [17]. It was shown (Fig. 2) that above the temperature T_1 of the first DSC peak, the nuclei with lithium tetragermanate $Li_2Ge_4O_9$ and lithium heptagermanate $Li_2Ge_7O_{15}$ structures appeared within the amorphous matrix. Above the second DSC peak (temperature T_2), the $Li_2Ge_4O_9$ nuclei disappeared and the thermodynamically stable $Li_2Ge_7O_{15}$ phase was crystallized completely.

3.2. Electrical conductivity

Temperature dependence of conductivity σ, measured on the first heating run of Li_2O–$7GeO_2$ as-quenched glass, is plotted in the Arrhenius scale in Fig. 3 [20]. One can see that dependence $\sigma(1/T)$ corresponds to nearly straight line on heating up to the glass transition point T_g (dependence 1 in Fig. 3). Near T_g, the glass softens and the slope of the $\sigma(1/T)$ dependence increases. In the interval between T_1 and T_2, the sample transforms to a partially crystallized intermediate state with increased conductivity (dependence 2 in Fig. 3). When the sample is heated above T_2, an abrupt and irreversible decrease of σ manifests a completion of the crystallization process

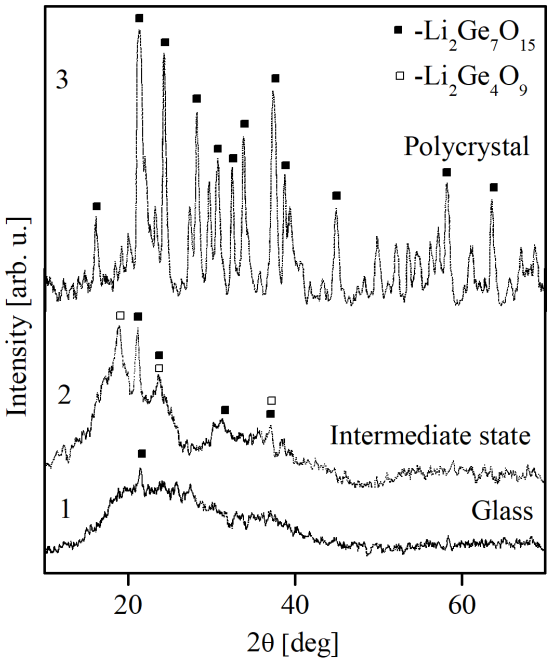

Fig. 2. X-ray diffractograms of Li_2O–$7GeO_2$ for glass (1), intermediate (2) and polycrysalline (3) states [17].

and a formation of $Li_2Ge_7O_{15}$ polycrystal (dependence 3 in Fig. 3) [17].

The data in Fig. 3 show that the electrical conductivity of the intermediate state exceeds by one and two orders of magnitude the expected σ values for glass and for polycrystal, respectively. This difference is even more pronounced and is about three orders of magnitude as compared with the conductivity of $Li_2Ge_7O_{15}$ single crystal (dependence 4 in Fig. 3). It should be noted that increase of conductivity on approaching T_g from below is usually observed for various amorphous solid electrolytes [21–24]. Nevertheless, as a rule, such growth of σ immediately followed by a sharp decrease because of glass crystallization. In our case, the increased conductivity is observed in a relatively wide temperature region between T_1 and T_2 as a result of staged crystallization process and presence of an intermediate state (Figs. 1, 3).

It is known that temperature increase of σ due to thermally activated processes can be described by expression

$$\sigma\,(T) = \frac{A}{T}\exp\left(\frac{-E_a}{k_B T}\right), \qquad (1)$$

where E_a represents the activation energy of conductivity, k_B is the Boltzmann constant, the coefficient $A = nq^2\delta^2\nu/(zk_B)$ depends on the carrier's concentration n, charge q, hopping length δ, frequency of the lattice vibrations ν, and the number z of nearest available positions.

As shown in [8–11], conductivity in $Li_2Ge_7O_{15}$ single crystals was mainly determined by interstitial Li^+ ions

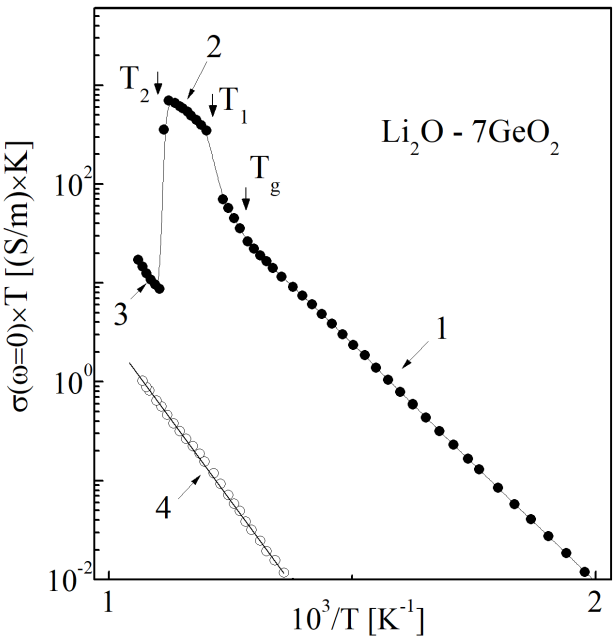

Fig. 3. Temperature dependence of conductivity plotted in the Arrhenius scale. Measurements were carried out for as-quenched Li_2O–$7GeO_2$ glass on the first heating run [20]. The indicated temperature ranges correspond to the following states: 1 — glass, 2 — intermediate state, 3 — polycrystalline state. The temperatures of DSC anomalies (see Fig. 1) are shown by arrows. For comparison the dependence (4) for $Li_2Ge_7O_{15}$ single crystal is added.

moving through the channels of Ge-O lattice framework. Study of $Li_2Ge_7O_{15}$ doped with Cr and Mn [9] gave evidence that σ growth on heating was governed by thermal activation of the Li^+ interstitials mobility. It is known that lithium heptagermanate is a typical dielectric with a bandgap width of 5.37 eV [25]. Accounting this fact and the data on σ kinetics in DC field, it was concluded [10] that above $\approx$ 500 K Li ionic transport gave a main contribution to charge transfer whereas electronic conductivity was negligible.

Comparison of the obtained results with the data of [8–11] enables to assume that charge transfer in glass, as well as intermediate and polycrystalline phases can be associated with Li^+ ions which are weakly bound to Ge–O structural framework and are able to hop through the quasi-equilibrium positions. One can see that activation energies for the intermediate and polycrystalline states can be determined for relatively narrow temperature intervals and, consequently, less accurately (Fig. 3). Nevertheless, comparison of the dependences slopes in Fig. 3 shows that activation energy for the intermediate state (0.80±0.04 eV) is noticeably lower than E_a values for the glass (0.95±0.01 eV) and polycrystalline samples (1.3±0.1 eV). Apparently, charge transfer in the intermediate state is accompanied by overcoming the lower potential barriers indicating a noticeable difference of its structure from the structures of glass and the polycrystalline state.

One should note that all σ changes (Fig. 3) are observed for the same chemical composition. Hence, increase of σ at T_1 and its subsequent sharp decrease at T_2 can be related to the features of atomic structure and/or morphology of the phase states studied. High σ in the interval between T_1 and T_2 can be considered as a result of high conductive phase formation and its spatial distribution. On the other hand, σ increase can be associated with the size of the ordered phase nuclei. The morphology of the samples in different states was examined by AFM.

3.3. Morphology of the states appearing at glass crystallization

The properties of the multiphase compounds strongly depend on the relative volume and shape of the homogeneous regions as well as on their spatial distribution. The morphology of the glass, intermediate and polycrystalline states was probed by AFM. To study morphology of the amorphous state, the cleavage surface was prepared for as-quenched glass. The sample in the intermediate state was prepared by heating as-quenched glass to the temperatures between the first and the second DSC peaks (Fig. 1) and by subsequent cooling to room temperature. The polycrystalline sample was prepared by heating glass above the second DSC peak (Fig. 1) with subsequent cooling to room temperature. For AFM imaging the samples in the intermediate and polycrystalline states, the cleavage surfaces were prepared after the heat treatment. Obviously that state of the samples was stable at room temperature and transformed only at much higher temperatures during heat treatment. Hence for used procedure, when cleavage planes were prepared on heat treated samples, the AFM images reflect the morphology of the states within the samples bulk. The AFM images obtained for the samples in glass, intermediate and polycrystalline states are shown in Fig. 4, where the light spots correspond to the regions with ordered structure.

The AFM data yield information on average size, geometry and distribution of ordered regions. Average sizes d of ordered regions and ordered phases fractions Δ are presented in Table I. After the mean values of d the widths of the size distributions are given in parentheses. The values of Δ were estimated from AFM images as ratio of total area occupied by nuclei to the area of studied surface. One can see that in glass state a small part of the sample surface is occupied by nanosized nuclei, which can be attributed to $Li_2Ge_7O_{15}$ phase in accordance with [17]. In the intermediate state, the nuclei are approximately twice larger and occupy about three quarters of the sample surface. In the polycrystalline samples, the crystallites with $Li_2Ge_7O_{15}$ structure [17] have an average size in micrometer range ($d \approx 0.3$ μm) and occupy nearly the whole sample surface.

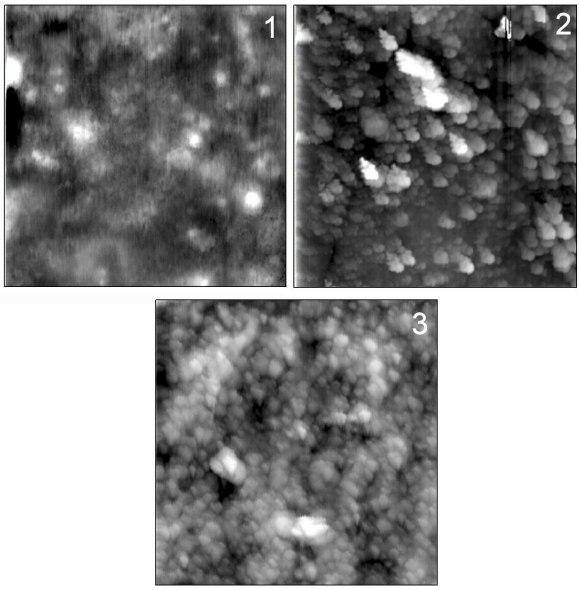

Fig. 4. AFM images illustrating morphology of the states obtained at Li_2O–$7GeO_2$ glass crystallization: 1 — glass, 2 — intermediate state, 3 — polycrystalline state. The investigated surface was 15×15 μm^2 .

TABLE I

Average linear size d of the nuclei/crystallites and ordered phase fraction Δ for the Li_2O-$7GeO_2$ states

The states of Li_2O–$7GeO_2$	d [nm]	Δ [%]
Glass	34 (14)	7
Intermediate nanocrystalline state	74 (33)	78
Polycrystalline state	293 (175)	93

Discussing the reasons for increased conductivity in the range between T_1 and T_2, one can note that the nanometer nuclei, appeared in the intermediate state, yield X-ray reflections characteristic for lithium tetragermanate and lithium heptagermanate structures (Fig. 2). We have no information on the results of conductivity measurements in lithium tetragermanate crystals. Nevertheless, accounting the data reported in [7], one can expect the conductivity of lithium tetragermanate close or slightly higher than σ of lithium heptagermanate. Thus, there is no basis to consider the phases, appearing in the range between T_1 and T_2, as highly conductive. Then, the σ increase in the intermediate state can be attributed to a nanometer-scale size of the ordered regions. In that case there should be a noticeable difference in the atomic potential reliefs of the nanocrystalline intermediate state on the one hand and glass and polycrystal on the other hand. Quantitatively this assumption can be supported by observed different slopes of the $\sigma(1/T)$ dependences in the range 2 compared with the intervals 1 and 3 in Fig. 3.

3.4. The mechanism of Li_2O–$7GeO_2$ glass crystallization

To understand the specific features of the intermediate state properties, it is important to know the mechanism of the amorphous phase crystallization. For this purpose we applied AFM to probe the morphology of Li_2O–$7GeO_2$ polycrystalline samples heat treated and prepared for experiment in different ways.

For the polycrystalline sample, shown in Fig. 4 (image 3), the procedure was as described in Sect. 3.3., i.e. heat treatment was performed first and then a cleavage surface for AFM imaging was prepared. For another sample this sequence was reversed, a cleavage surface was prepared for as-quenched glass. After that this sample was treated to the polycrystalline state by heating above T_2 and subsequently cooled to room temperature. The morphology of the sample prepared in this way is shown in Fig. 5.

Comparison of the data given in Fig. 4 (image 3) and Fig. 5 shows that sequence of heat treatment and cleavage surface preparation significantly affects the samples morphology observed by AFM. In Fig. 4 (image 3), an almost complete ordering of the structure is observed and the crystallites with an average linear size of about 0.3 μm occupy more than 90% of the total surface area (Table I). For the sample, AFM image of which is shown in Fig. 5, crystallites with an average linear size of $\approx$ 40 nm occupy about 20% of the total surface area.

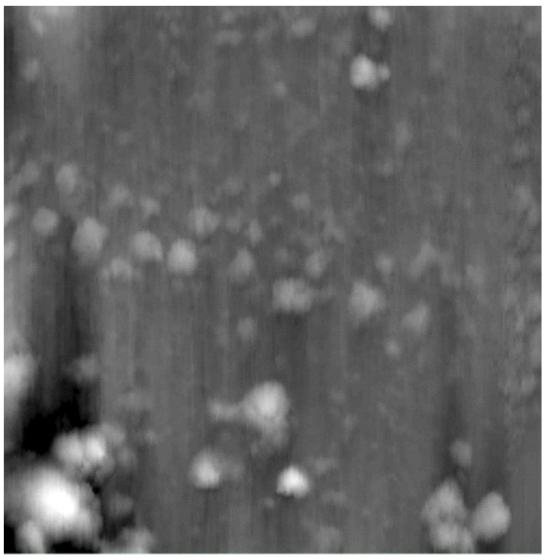

Fig. 5. AFM image showing Li_2O–$7GeO_2$ glass crystallization near the samples surface (15×15 μm^2) .

As it was shown in [18, 19], the state of the samples below glass transition point T_g practically did not change. Glass could be transformed to polycrystal by heating to $T>T_2$ or by isothermal treating for certain time above T_g. This means that the AFM image 3 in Fig. 4 visualizes a crystallization pattern within the samples bulk, whereas AFM data shown in Fig. 5 demonstrate crystallization near the samples surface. Thus, the AFM data give evidence that Li_2O–$7GeO_2$ glass crystallizes in the samples

bulk. Nucleation and growth of the ordered regions turns out to be suppressed near the samples surface.

4. Conclusions

Electric conductivity in AC field was studied during crystallization of Li_2O–$7GeO_2$ glass on heating. It was shown that amorphous phase crystallized in stages through formation of intermediate state with increased conductivity, as compared with glass and polycrystalline states. According to AFM data, the intermediate state was characterized by the appearance of nanometer-sized ordered regions. On subsequent heating nanometer-sized nuclei transformed into micrometer-sized crystallites, complete crystallization was accompanied by sharp decrease of electric conductivity. The AFM study showed that Li_2O–$7GeO_2$ glass crystallized within the sample bulk, whereas near the sample surface the amorphous state was stabilised. Charge transfer in Li_2O–$7GeO_2$ multiphase compounds is attributed to a motion of Li ions, which are weakly bound to Ge–O structural framework. Obtained data demonstrate that a creation of spatially inhomogeneous multiphase media can be an effective approach to increase ionic conductivity in dielectrics.

References

[1] J. Maier, *Solid State Ion.* **175**, 7 (2004).

[2] J. Maier, *Nature Mater.* **4**, 805 (2005).

[3] K. Murthy, *J. Am. Ceram. Soc.* **47**, 328 (1964).

[4] H. Vollenke, A. Wittman, H. Nowotny, *Monatch. Chem.* **101**, 46 (1970).

[5] Y. Iwata, I. Shibuya, M. Wada, A. Sawada, Y. Ishibashi, *J. Phys. Soc. Jpn.* **56**, 2420 (1987).

[6] G.D. Ilyushin, L.N. Dem'yanets, *Crystallogr. Rep.* **45**, 626 (2000).

[7] B.E. Liebert, R.A. Huggins, *Mater. Res. Bull.* **11**, 533 (1976).

[8] M.D. Volnyanskii, M.P. Trubitsyn, Y.A.H. Obaidat, *Phys. Solid State* **50**, 422 (2008).

[9] M.P. Trubitsyn, M.D. Volnyanskii, Y.A.H. Obaidat, *Phys. Solid State* **50**, 1234 (2008).

[10] M.D. Volnyanskii, S.N. Plyaka, M.P. Trubitsyn, Y.A.H. Obaidat, *Phys. Solid State* **54**, 499 (2012).

[11] M. Volnianskii, S. Plyaka, M. Trubitsyn, Y. Obaidat, *Ferroelectrics* **462**, 74 (2014).

[12] P. Pernice, A. Aronne, M. Marotta, *Mater. Chem. Phys.* **30**, 195 (1992).

[13] P. Pernice, A. Aronne, M. Marotta, *J. Mater. Sci. Lett.* **11**, 427 (1992).

[14] A. Marotta, P. Pernice, A. Aronne, M. Catauro, *J. Therm. Anal.* **40**, 181 (1993).

[15] A. Aronne, M. Catauro, P. Pernice, A. Marotta, *Thermochim. Acta* **216**, 169 (1993).

[16] M.D. Volnyanskii, A.A. Nesterov, M.P. Trubitsyn, *Phys. Solid State* **54**, 945 (2012).

[17] M.D. Volnianskii, O.O. Nesterov, M.P. Trubitsyn, *Ferroelectrics* **466**, 126 (2014).

[18] O.O. Nesterov, M.P. Trubitsyn, D.M. Volnyanskii, *Phys. Solid State* **57**, 683 (2015).

[19] O.O. Nesterov, M.P. Trubitsyn, S.N. Plyaka, D.M. Volnyanskii, *Phys. Solid State* **57**, 1759 (2015).

[20] O.O. Nesterov, M.P. Trubitsyn, S.M. Plyaka, M.D. Volnyanskii, *Visnik Dnipropetrovs'kogo uněversitetu. Seria fizika, radioelektronika* **22**, 117 (2015).

[21] St. Adams, K. Hariharan, J. Maier, *J. Solid State Phenom.* **39-40**, 285 (1994).

[22] B.K. Money, K. Hariharan, *J. Phys. Condens. Matter* **21**, 1 (2009).

[23] J. Fu, *Solid State Ion.* **104**, 191 (1997).

[24] M.L.F. Nascimento, *Electrochemistry* **2013**, 1 (2013).

[25] S. Haussuhle, F. Wallrafen, K. Recker, J. Eckstein, *Z. Kristallogr.* **153**, 329 (1980).